A haemocompatible and scalable nanoporous adsorbent monolith synthesised using a novel lignin binder route to augment the adsorption of poorly removed uraemic toxins in haemodialysis



2017 Biomed. Mater. 12 035001

(http://iopscience.iop.org/1748-605X/12/3/035001)

Biomedical Materials

PAPER

# A haemocompatible and scalable nanoporous adsorbent monolith synthesised using a novel lignin binder route to augment the adsorption of poorly removed uraemic toxins in haemodialysis

**Susan R Sandeman**[1], **Yishan Zheng**[1], **Ganesh C Ingavle**[1], **Carol A Howell**[1], **Sergey V Mikhalovsky**[1], **Kolitha Basnayake**[2], **Owen Boyd**[3], **Andrew Davenport**[4], **Nigel Beaton**[5] **and Nathan Davies**[5]

[1] Biomaterials and Medical Devices Research group, School of Pharmacy and Biomolecular Sciences Huxley Building, University of Brighton, Brighton, BN2 4GJ, United Kingdom
[2] Sussex Kidney Unit, Brighton & Sussex University Hospitals NHS Trust, Brighton, BN2 5BE, United Kingdom
[3] Intensive Care Unit, Brighton & Sussex University Hospitals NHS Trust, Brighton, BN2 5BE, United Kingdom
[4] UCL Centre for Nephrology, Royal Free Campus, Roland Hill Street, London NW3 2PF, United Kingdom
[5] UCL Institute for Liver and Digestive Health, Royal Free Campus, Roland Hill Street, London NW3 2PF, United Kingdom

**E-mail:** s.sandeman@brighton.ac.uk

**Keywords:** nanoporous, end stage renal disease, haemodialysis, uraemic toxins, activated carbon, monolith

OPEN ACCESS

RECEIVED
4 November 2016

REVISED
27 February 2017

ACCEPTED FOR PUBLICATION
8 March 2017

PUBLISHED
10 May 2017



## Abstract

Nanoporous adsorbents are promising materials to augment the efficacy of haemodialysis for the treatment of end stage renal disease where mortality rates remain unacceptably high despite improvements in membrane technology. Complications are linked in part to inefficient removal of protein bound and high molecular weight uraemic toxins including key marker molecules albumin bound indoxyl sulphate (IS) and p-cresyl sulphate (PCS) and large inflammatory cytokines such as IL-6. The following study describes the assessment of a nanoporous activated carbon monolith produced using a novel binder synthesis route for scale up as an in line device to augment haemodialysis through adsorption of these toxins. Small and large monoliths were synthesised using an optimised ratio of lignin binder to porous resin of 1 in 4. Small monoliths showing combined significant IS, p-CS and IL-6 adsorption were used to measure haemocompatibility in an *ex vivo* healthy donor blood perfusion model, assessing coagulation, platelet, granulocyte, T cells and complement activation, haemolysis, adsorption of electrolytes and plasma proteins. The small monoliths were tested in a naive rat model and showed stable blood gas values, blood pressure, blood biochemistry and the absence of coagulopathies. These monoliths were scaled up to a clinically relevant size and were able to maintain adsorption of protein bound uraemic toxins IS, PCS and high molecular weight cytokines TNF-$\alpha$ and IL-6 over 240 min using a flow rate of 300 ml $min^{-1}$ without platelet activation. The nanoporous monoliths where haemocompatible and retained adsorptive efficacy on scale up with negligible pressure drop across the system indicating potential for use as an in-line device to improve haemodialysis efficacy by adsorption of otherwise poorly removed uraemic toxins.

## 1. Introduction

Nanoporous adsorbents offer a potential method by which to address the life-reducing complications associated with poor removal of protein bound and high molecular weight uraemic toxins during haemodialysis. Whilst more than two million patients with end stage renal disease (ESRD) are treated by haemodialysis worldwide mortality rates remain high. Almost half of all patients who receive a diagnosis of ESRD die within three years, most commonly as a result of cardiovascular co-morbidity followed by infection [1–4]. Haemodialysis is a life sustaining therapy and an efficient method for removing excess fluid and highly water soluble small molecules such as ionic solutes and urea from blood. Urea is known to hydrolyse into cyanate and form carbamylated haemoglobin [5–8] and other carbamylated proteins and lipoproteins. However, there is debate as to whether urea is a 'uraemic' toxin or whether its use as a marker

of dialysis adequacy actually correlates with adequate removal of uraemic toxins with the most damaging effects on tissue physiology [9, 10]. Urea is rapidly cleared during standard haemodialysis whereas other uraemic retention solutes, particularly protein bound and high molecular weight molecules, are minimally cleared resulting in retention in ESRD patients [11]. Indoxyl sulphate (IS) and p-cresyl sulphate (PCS) are protein bound uraemic toxins derived from protein metabolism [12]. They have been shown, both within *in vitro* and in animal models, to cause endothelial damage and cardiovascular disease, and are associated with increased mortality in ESRD patients [12–17]. To date a suitable method to remove these and the many other poorly removed protein bound and high molecular uraemic toxins [17] remains to be found [11, 18].

Addition of an adsorption device into the standard haemodialysis circuit has great potential to improve removal of such toxins [2, 19–23]. Synthetic, activated carbon adsorbents offer considerable advantages over other polymer based systems. They outperform other adsorbents through the existence of a highly developed internal surface area which is suitable for non-specific adsorption of predominantly hydrophobic, organic molecules. Early studies using various granular AC formulations from a range of natural sources showed some success but were ultimately constrained by variable performance, poor haemocompatibility particularly related to platelet loss, pressure drop and poor adsorption of larger biological molecules when coated [24–31]. Advances in production technology using synthetic pre-cursors have improved activated carbon performance through carefully controlled formulation, carbonisation and activation procedures allowing the production of mechanically strong microbeads with an internal surface area of over 1500 $m^2 g^{-1}$ [32–34]. Additionally it is possible to significantly increase capacity for the removal of protein bound and high molecular weight uraemic toxins through the development of nanopores with diameter in the range of 10–100 nm [35–38]. This structure can be maintained and potential for pressure drop reduced by the production of activated carbon monoliths, formed as extruded cylinders with numerous micro-diameter channels along which blood flows. We have previously shown that nanoporous activated carbon monoliths can adsorb protein bound uraemic and high molecular weight toxins which are poorly removed by haemodialysis alone [39]. However, a monolith synthesis route which enabled the production of monoliths with attrition resistance and adsorptive capacity on scale up to a clinically relevant size was not possible using the previous synthesis route. The aim of the current study was to assess monoliths produced by a novel lignin binder route for haemocompatibility using *ex vivo* healthy donor and a niave rat haemoperfusion model. Maintenance of nanoporosity and adsorptive capacity on scale up was then assessed with the ultimate goal of providing a potential augmentation strategy for haemodialysis.

## 2. Materials and methods

### 2.1. Monolith synthesis

Monoliths were synthesised using a novolac phenol-formaldehyde resin pre-cursor dissolved in a pore-forming solvent, ethylene glycol, together with a cross-linking agent, hexamethylenetetramine, and lignin binder. The ratio of lignin binder to nanoporous resin was optimised to a wt% ratio of 25:75. The pre-polymer solution was cured and the resulting resin cake was crushed, washed and dried to remove excess pore former then milled and formed into a dough for extrusion. The resulting monoliths were carbonised at 700 °C and activated in carbon dioxide at temperatures of up to 880 °C. Nanoporosity was controlled primarily by initial resin pore-former composition and the unique phase separation that occurs during the curing stage. Small monoliths were prepared with a diameter of 7 mm, length of 95 mm and contained 30 square micro-channels. Large monoliths were prepared with a diameter of 30 mm and length of 225 mm and contained 600 square micro-channels with a diameter of 300 $\mu$m. The monoliths were encased in heat shrink polyolefin tubes supplied by RS Components Ltd (Northamptonshire, UK). The process sealed Leuer lock fittings to the ends of the monoliths prior to the perfusion studies (figures 1(a) and (b)).

### 2.2. Physical characterisation of small and large monoliths

The surface and internal porous morphology of the resultant monolithic materials were characterised by scanning electron microscopy (SEM) using a Sigma field emission gun-SEM microscope (Carl Zeiss NTS, Cambridge, UK). The definition of pore size in nanoporous materials according to the International Union of Pure and Applied Chemistry is that micropores are smaller than 2 nm in diameter, mesopores 2–50 nm and macropores larger than 50 nm. The carbons used in this study were predominantly micro-macroporous. Prior to measurement, the hierarchically porous monolithic materials were dried under vacuum at 150 °C overnight. The pore size distribution data was determined using a PoreMaster mercury intrusion porosimeter (Quantachrome Instruments Ltd, Hook, UK). Surface area was determined using an Autosorb-1 gas sorption analyser, (Quantachrome Instruments, USA) using Quantachrome data analysis software (Quantachrome ASiQwin) and the Brunauer, Emmett and Teller (BET) method.

### 2.3. Adsorption of marker uraemic toxins by the small monoliths

The small monoliths were primed with saline solution for 30 min at a flow rate of 5 ml $min^{-1}$. A 20 ml

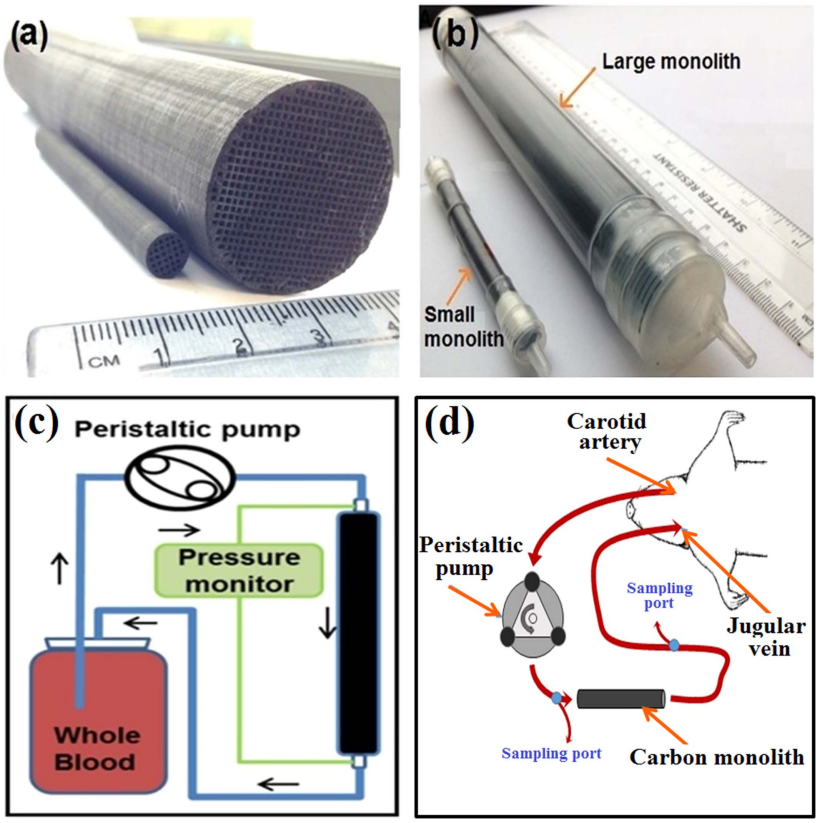


**Figure 1.** (a) Small and large monoliths were produced using a novel lignin binder route with dimensions of 0.7 cm × 9.5 cm and 2.8 × 22.5 cm (diameter by length) and microchannel numbers of 30 channels and 600 channels respectively. (b) The monoliths were encased in heat shrink polyolefin tubes. (c) *In vitro* plasma and whole blood experiments were conducted, perfusing fluid through the monolith microchannels at a flow rate of 5 ml $min^{-1}$ for the small monolith studies and 300 ml $min^{-1}$ for the large monolith studies. (d) A naive rat haemoperfusion model was used to carry out an *in vivo* safety assessment of the small monoliths.

volume of fresh frozen human plasma (Cambridge Bioscience) was spiked with IS (125 $\mu$M), PCS (250 $\mu$M) and IL6 (1 ng $ml^{-1}$). The spiked plasma solution underwent continuous circulation through the monoliths and samples were collected over time. IS and PCS concentrations were measured by HPLC using a method described in [39] and IL6 concentration was measured by ELISA according to manufacturer's instructions using a plasma dilution of 1:5 (BD Biosciences).

### 2.4. Haemocompatibility testing of small monoliths

Haemocompatibility studies were carried out according to ISO standard 10993-4:2002 (E) using freshly drawn healthy donor blood from an anonymised healthy donor database held by the NIHR Brighton & Sussex Clinical Research Facility using informed consent protocols (UK National Research Ethics System (NRES) Committee South East Coast—Brighton and Sussex REC reference 13/LO/1058). The small monoliths (7 mm × 95 mm with 30 micro-channels) were pre-conditioned with saline (0.9% NaCl) for 30 min prior to continuous circulation of 20 ml of healthy donor blood through the monoliths for 60 min at a flow rate of 5 ml $min^{-1}$ (figure 1(c)). Plasma was prepared by centrifugation of blood samples at 3500 rpm for 15 min.

### 2.5. Complement activation

The presence of C3a, C4a and C5a was measured in plasma prepared from EDTA anticoagulated blood by enzyme linked immunosorbent assay (ELISA) (BD Biosciences). ELISAs were carried out according to manufacturer's instructions issuing a 1 in 2000 dilution for C3a and C4a and a 1 in 40 dilution for C5a.

### 2.6. Platelet activation

The presence of PAC-1 and CD62 platelet activation markers (BD Biosciences UK) was measured in sodium citrate anticoagulated donor blood samples pre- and post- perfusion through monolith and tubing only controls using flow cytometry. The first 2 ml blood was drawn and discarded. 2 ml of blood incubated with ADP (2 $\mu$M) (Sigma Aldrich, UK) for 5 min was used as a positive control. Fresh whole blood samples (5 $\mu$l) were incubated in the dark with PE/CD61 (10 $\mu$l), allophycocyanin (APC)/D62P (10 $\mu$l) and fluorescein isothiocyanate (FITC)/PAC-1 (10 $\mu$l) antibody cocktail for 20 min, fixed using chilled 1% paraformaldehyde in PBS (1 ml) for 30 min at 4 °C and analysed using an Accuri C6 flow

cytometer and BD CSampler software (version 1.0.264.21). The flow cytometer was set to slow flow rate, with a forward scatter (FSC) threshold of 10 000 to collect 10 000 events on the platelet gate.

### 2.7. Granulocyte activation

Granulocyte activation was measured by testing lithium heparin anticoagulated donor blood samples for the presence of CD14/CD11b markers (Biolegend, UK) using flow cytometry. Positive control samples were prepared by incubating blood samples with interleukin 6 (IL-6) (50 ng ml$^{-1}$) and interleukin 8 (IL-8) (50 ng ml$^{-1}$) for 60 min. Blood samples (100 $\mu$l) were incubated with PE/CD14 (20 $\mu$l) and APC/CD11b (20 $\mu$l) antibody cocktails for 20 min. Stained blood samples were incubated with lyse/fix buffer (1.5 ml) in the dark for 30 min prior to centrifugation at 600 g for 6 min, removal of supernatant and washing of cells in 2 ml stain buffer. Cells were pelleted and resuspended in 300 $\mu$l stain buffer for analysis using flow cytometry. The flow cytometer was set to medium flow rate, with a FSC threshold of 80 000 to collect 10 000 events.

### 2.8. T cell activation

T cell activation was assessed in EDTA anticoagulated blood samples by measuring the activation of STAT3 and STAT5 intracellular phosphorylation pathways using flow cytometry. Whole blood samples (200 $\mu$l) were lysed, permeabilised and stained by incubating with PerCP/CD3, Alexa488/CD8, PE/CD4 antibody cocktail (20 $\mu$l) and Alexa647/STAT3 or STAT5 (20 $\mu$l) for 1 h. Positive control samples were prepared using an IL-6 (50 ng ml$^{-1}$) and IL-8 (50 ng ml$^{-1}$) spike for STAT3 activation and interleukin 2 (IL-2) (50 ng ml$^{-1}$) spike for STAT5 activation followed by incubation for 60 min. Cells were washed and resuspended in 200 $\mu$l stain buffer for analysis using flow cytometry with setting as for the granulocyte activation assay.

### 2.9. Adsorption of uraemic toxins by the large monoliths

Large monoliths ($n = 3$) were pre-conditioned with intravenous infusion saline solution (0.9% NaCl, 0.15% KCl and 0.2% MgCl) (Baxter) for 30 min. A 400 ml volume of blood, anti-coagulated with sodium heparin and commercially supplied by Cambridge Biosciences, was spiked with 1000 pg ml$^{-1}$ IL-6 and tumor necrosis factor alpha (TNF-$\alpha$), 125 $\mu$M IS and 250 $\mu$M PCS and continuously perfused through the monolith or tubing controls for 60 min at a flow rate of 300 ml min$^{-1}$ (LaboVAR 225 pump, Möller Medical GmbH Fulda Germany). Samples were collected after 0, 5, 15, 30, 45, 60, 90 min. A second study extended sampling to 240 min. IS and PCS concentrations were measured by HPLC using a method described in [39] and IL6/TNF-$\alpha$ concentration was measured by ELISA according to manufacturer's instructions using a dilution of 1:5 (BD Biosciences). Platelet activation was measured in the plasma derived from the timed blood samples as described in section 2.5.

### 2.10. *In vivo* safety assessment of small monoliths

All studies were conducted under the governance of the UK Animals in Scientific Procedures Act (1986, amended 2012), with full local ethical approval. Animals were allowed free access to food and water prior to the study and housed under a 12 h light/dark cycle at 20 °C (±2 °C). Adult male Sprague-Dawley rats (250–300 g, Charles River UK) were anaesthetised under isofluorane (induction at 5% in oxygen, maintenance at 1.5% in air for the duration of the study) and had catheters placed in the left carotid artery and right jugular vein. Mean arterial pressure was recorded at hourly intervals (Biopac US) and core body temperature recorded throughout the study. To maintain body temperature, the animals were maintained on regulated heat mats and covered with insulated materials as required.

Blood samples were collected into lithium heparin coated tubes for blood gas analysis (Siemens Medical Diagnostics, UK) and plasma biochemistry prior to, and at hourly intervals throughout the study. After an initial 30 min stabilisation period, the arterial catheter was connected to a carbon monolith (approximately 10 cm by 1 cm (length × diameter)) via a peristaltic pump (figure 1(d)). The blood was then returned to the animal via the catheter placed into the jugular vein. Flow rates throughout the 2 h treatment period were set at 2 ml min$^{-1}$ with the total circuit volume not exceeding 10% of the circulating blood volume of the animal (ca 3 ml maximum). The circuit was pre filled with heparinised saline solution (1000 U l$^{-1}$), with a saline bolus (ca 2 ml) administered to the animal at the start of treatment to prevent hypotension. At the termination of the study, blood and tissue samples were collected under terminal anaesthesia. Blood samples for biochemistry were stored on ice before centrifugation (3500 rpm, 10 min, 4 °C) and storage at −80 °C. Plasma biochemistry (glucose, urea, albumin, total protein, ALT, AST, creatinine) was assessed using an automated COBAS system (Roche, UK) following manufacturer's instructions.

### 2.11. Statistical analysis

Statistical analysis was carried out using GraphPad Prism 6.05 software and two-way ANOVA with Tukey's multiple comparison tests.

## 3. Results

### 3.1. Physical characterisation of the large and small monoliths

The synthesis and activation process resulted in a well-defined distribution of transport microchannels

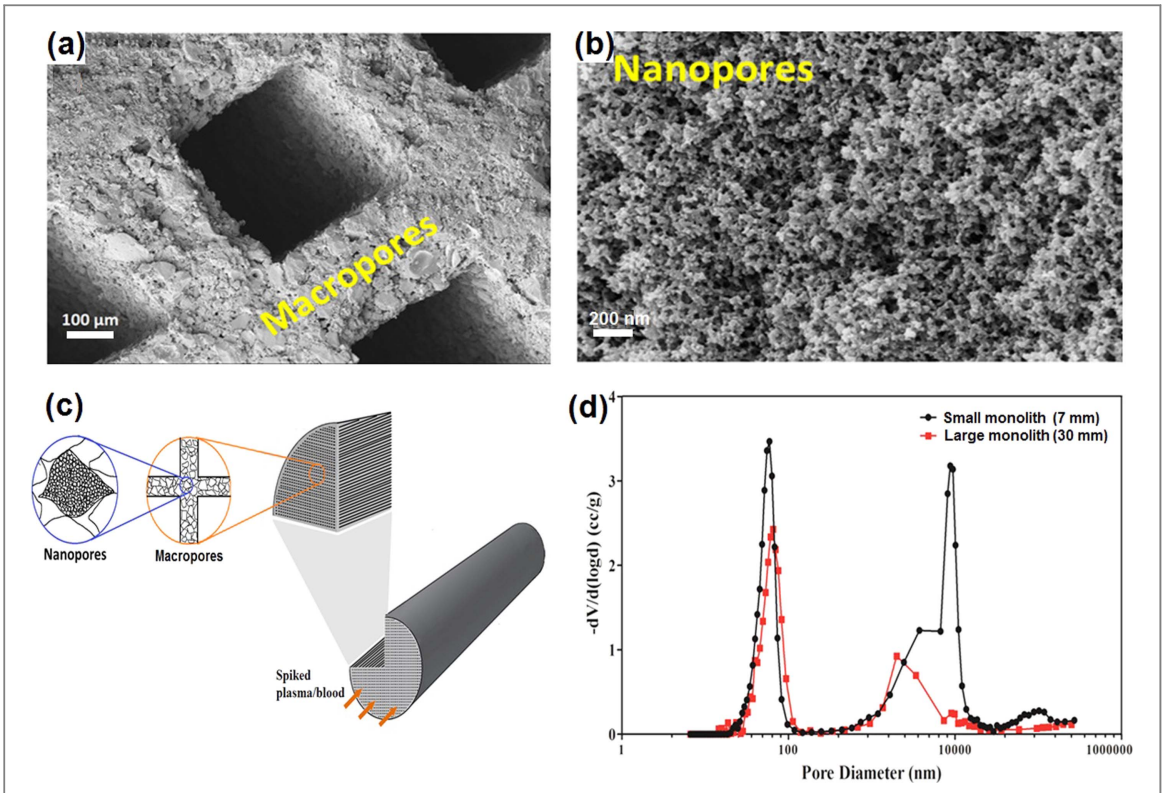


**Figure 2.** (a) Scanning electron micrograph showing microchannel geometry and (b) nanoporous domains within the walls of the small and large monoliths. (c) Mercury pore size distribution plots indicated consistent meso-macroporosity in the small and large monoliths with a mean pore size of 56 nm and 62 nm respectively and $S_{BET}$ surface area calculated by gas nitrogen porosimetry of 1117 and 1056 $m^2\ g^{-1}$ respectively.

running in parallel along the length of the monoliths (figures 2(a)–(c)). The internal structure of the carbon monolith walls was visible in the SEMs as larger macroporous and smaller nanoporous domains. The mercury porosimetry pore size distribution plot indicated nanoporous domains in the 20–100 nm range in both the small and large monoliths with mean peak porosity of 55.6 nm and 62.1 nm respectively (figure 2(d)). The BET surface area was calculated by gas nitrogen porosimetry to be 1117 $m^2\ g^{-1}$ in the small monoliths and 1056 $m^2\ g^{-1}$ in the large monoliths.

### 3.2. Adsorption of marker uraemic toxins by the small monoliths

The small monoliths synthesised using a 25% lignin binder were able to adsorb uraemic toxins IS and PCS, reducing them to neglible levels and reduced IL-6 concentration by 80% (figure 3).

### 3.3. Haemocompatibility testing of the small monoliths

*3.3.1. Complement activation*

Blood perfused through the small monoliths over time did not cause significant complement activation when compared to the negative, tubing only control ($p > 0.05$) (figures 4(a)–(c)). Some complement activation was observed at baseline and a slight increase occurred in both the monolith and tubing only controls over the 60 min perfusion cycle. However, this was significantly less than that of the zymosan A activated positive controls in which complement fragment concentrations increased from 1.5 to 4.1 ng $ml^{-1}$ for C3a ($p < 0.0001$) (figure 4(a)), 1.6 to 3.3 ng $ml^{-1}$ for C4a ($p < 0.05$) (figure 4(b)) and 3.9 to 43.5 pg $ml^{-1}$ for C5a ($p < 0.0001$) (figure 4(c)). C5a concentration detected in the plasma was in the picogram range and significantly lower than that for C3a and C4a which was in the ng range.

*3.3.2. Platelet activation*

A platelet sub-population was isolated from the total blood cell population using a R-Phycoerythrin (PE) fluorophore conjugated CD61 antibody against the platelet surface antigen glycoprotein IIIa. Within this platelet sub-population activated platelets were detected using a FITC fluorophore conjugated PAC-1 antibody and an APC conjugated CD62p antibody (figures 4(d) and (e)). No significant platelet activation occurred following 60 min of perfusion through the small monoliths and the tubing only controls. No significant difference in the percentage of PAC-1 and CD62P positive platelets was observed when comparing the monolith and tubing only control following 60 min continuous filtration through the *ex vivo* circuit. In contrast, the PMA (200 nM) spike induced significant platelet activation (SEM±, $n = 3$, $p < 0.0001$).

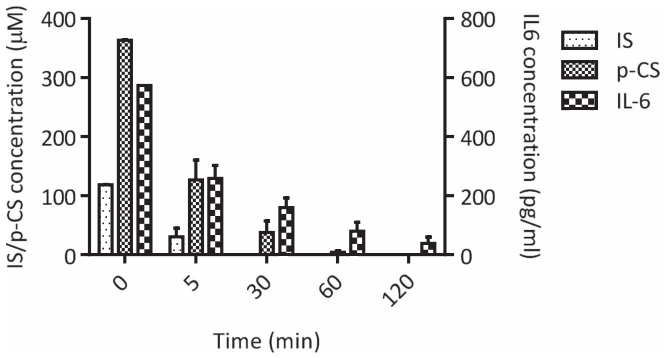


**Figure 3.** Adsorption of IS (125 $\mu$M), p-CS (250 $\mu$M) and IL-6 (1000 pg ml$^{-1}$) from spiked fresh frozen human plasma over time by the small monoliths synthesised using a 25:75%wt ratio of lignin to nanoporous resin ($n = 3$, mean $\pm$ SEM).

*3.3.3. Granulocyte activation*

No significant difference in granulocyte activation was observed between the monolith and tubing only controls following 60 min perfusion, although granulocyte activation did occur in both circuits (data not shown). Granulocyte activation, measured by elevated CD11b expression, occurred over 30 and 60 min blood perfusion through both monoliths and control but was less than that measured in the cytokine stimulated positive control (SEM$\pm$, $n = 3$). 8% granulocyte activation was measured at baseline, 20 $\pm$ 4% after 30 min perfusion and 70 $\pm$ 13% after 60 min perfusion in both the small monolith and tubing only samples.

*3.3.4. T cell activation*

The PE conjugated CD3 antibody was used to identify the T cell subpopulation. Alexa 647 conjugated STAT3 and STAT5 antibodies were used to identify the post-perfusion, activated T cells, IL6/IL8 (50 ng ml$^{-1}$) activated STAT3 positive control and IL2 activated STAT5 positive control (figures 4(f) and (g)). No up regulation of intracellular STAT phosphorylation pathways was detected following blood perfusion through the small monoliths over 60 min. Negligible levels of STAT3 phosphorylation and STAT5 phosphorylation and levels of 10%–20% were detected in the pre- and post-perfusion monolith samples, tubing only control samples and time 0 cytokine spiked positive controls. A significant increase in the cytokine stimulated positive control samples occurred over 60 min. 91 $\pm$ 3% STAT5 T-cell activation and 64 $\pm$ 2% STAT3 T-cell activation was detected. No significant T cell activation, measured by phosphorylated STAT3 and STAT5 protein expression, was observed following blood perfusion through the monoliths over 60 min compared to the cytokine (50 ng ml$^{-1}$) stimulated controls (SEM$\pm$, $n = 3$, $p < 0.0001$).

*3.3.5. Blood biochemistry and coagulometry*

Haemoglobin and haematocrit values, blood cell count, ionic solutes, urea, creatinine, total protein, albumin, fibrinogen and coagulometry measures remained in normal range and were not removed significantly by blood perfusion through the small monoliths (table 1). Limited reduction in platelet count, total protein and albumin concentration occurred following blood perfusion through the monoliths. Platelet count dropped from 261 $\pm$ 54 to 230 $\pm$ 75 $\times$ 109 cells ml$^{-1}$ post-monolith perfusion. The total protein concentration dropped from 75.7 $\pm$ 2.5 to 64 $\pm$ 2 g l$^{-1}$ and albumin concentration dropped from 46 $\pm$ 1 to 39.7 $\pm$ 0.6 g l$^{-1}$, all remaining in normal concentration range. A significant reduction in creatinine concentration occurred, reducing from 66.7 $\pm$ 13.6 to 17.7 $\pm$ 6 $\mu$mol l$^{-1}$. No change in activated partial thromboplastin times (APPT) or International normalised ratio (INR) were observed. Fibrinogen concentration reduced from 2.8 g l$^{-1}$ in the pre-perfusion blood samples to 2.1 g l$^{-1}$ in the monolith post perfusion samples but remained within the normal reference range.

### 3.4. Adsorption of uraemic toxins by the large monoliths

IS and PCS concentrations were reduced from 125 and 250 $\mu$M to negligible levels following perfusion through the large, 30 mm diameter monoliths for 90 min compared to the tubing only positive controls where IS and PCS concentration remained unchanged (figures 5(a)–(d)). The monoliths adsorbed IL-6 and TNF-$\alpha$, significantly reducing IL-6 concentration from 711 to 162 pg ml$^{-1}$ and TNF-$\alpha$ from 1070 to 441 pg ml$^{-1}$ over a 90 min perfusion cycle. A platelet activation study showed no significant activation of platelets over 90 min of perfusion through the monoliths and controls (figure 6). A further study extending the perfusion cycle to 240 min showed continued reduction in IS, PCS and IL-6 (figure 7).

### 3.5. *In vivo* safety assessment of small monoliths

The *in vivo* monolith perfusion safety study indicated no major concerns with regard to biocompatibility. None of the studies conducted showed any evidence of coagulopathies, either in terms of excess bleeding or clotting abnormalities. The circuit was pre-filled with

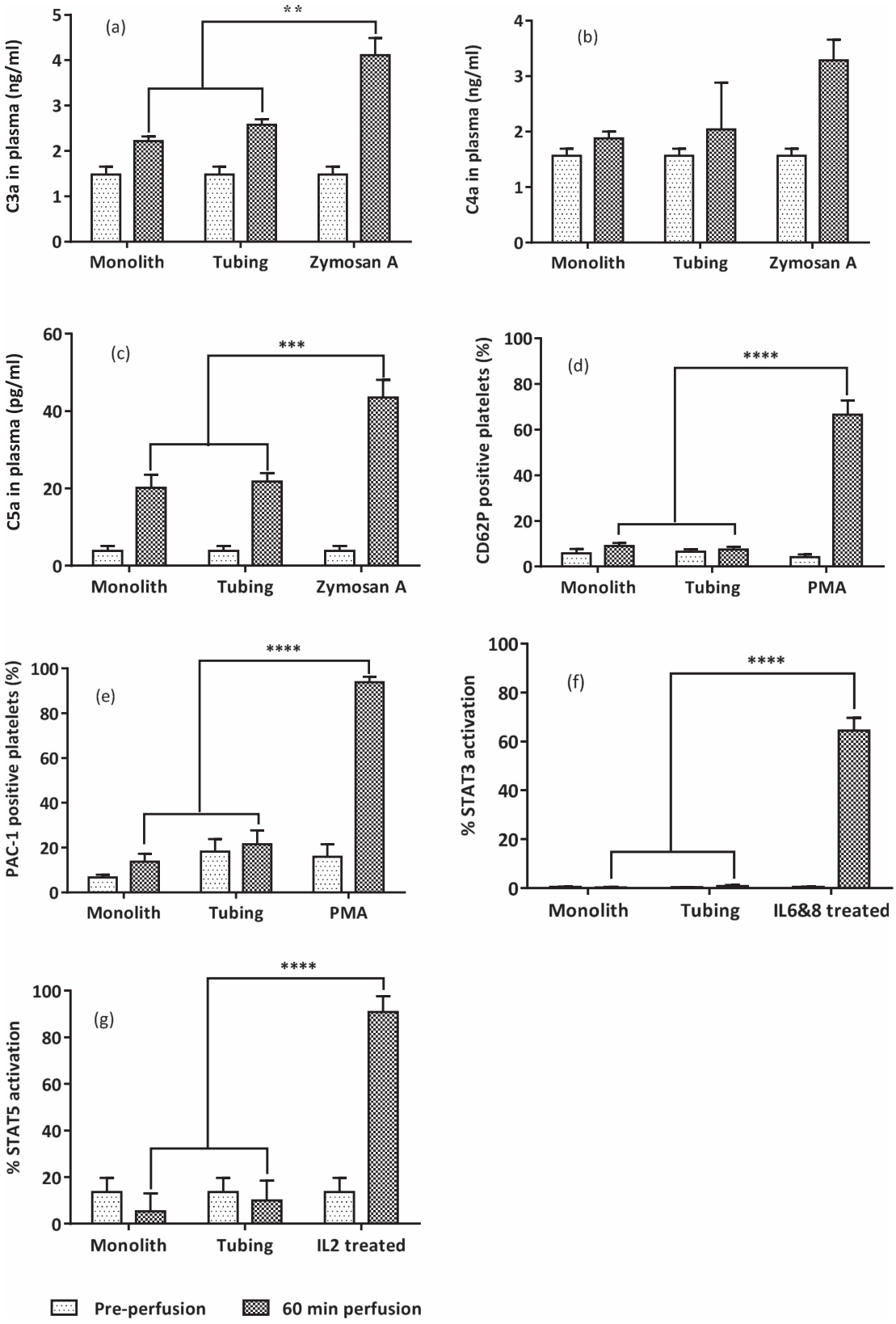


**Figure 4.** Perfusion of freshly drawn healthy donor blood through the small monoliths over 60 min stimulated no significant complement activation measured using (a) C3a (b) C4a and (c) C5a activation markers, no significant platelet activation measured using (d) PAC-1 and (e) CD62P activation markers and no significant T cell activation, measured using phosphorylated (f) STAT3 and (g) STAT5 protein expression when compared to tubing only controls in comparison to the zymosan A, PMA and cytokine stimulated positive controls (mean ± SEM, $n = 3$), $^{**}p < 0.01$, $^{****}p < 0.0001$.

heparinised saline, thought there was no evidence that the monolith removed heparin form the circuit. Blood gas values remained stable throughout the duration of the study (table 2), with only the bicarbonate level showing a moderate decline over the two-hour treatment period. This may be due to the amount of saline

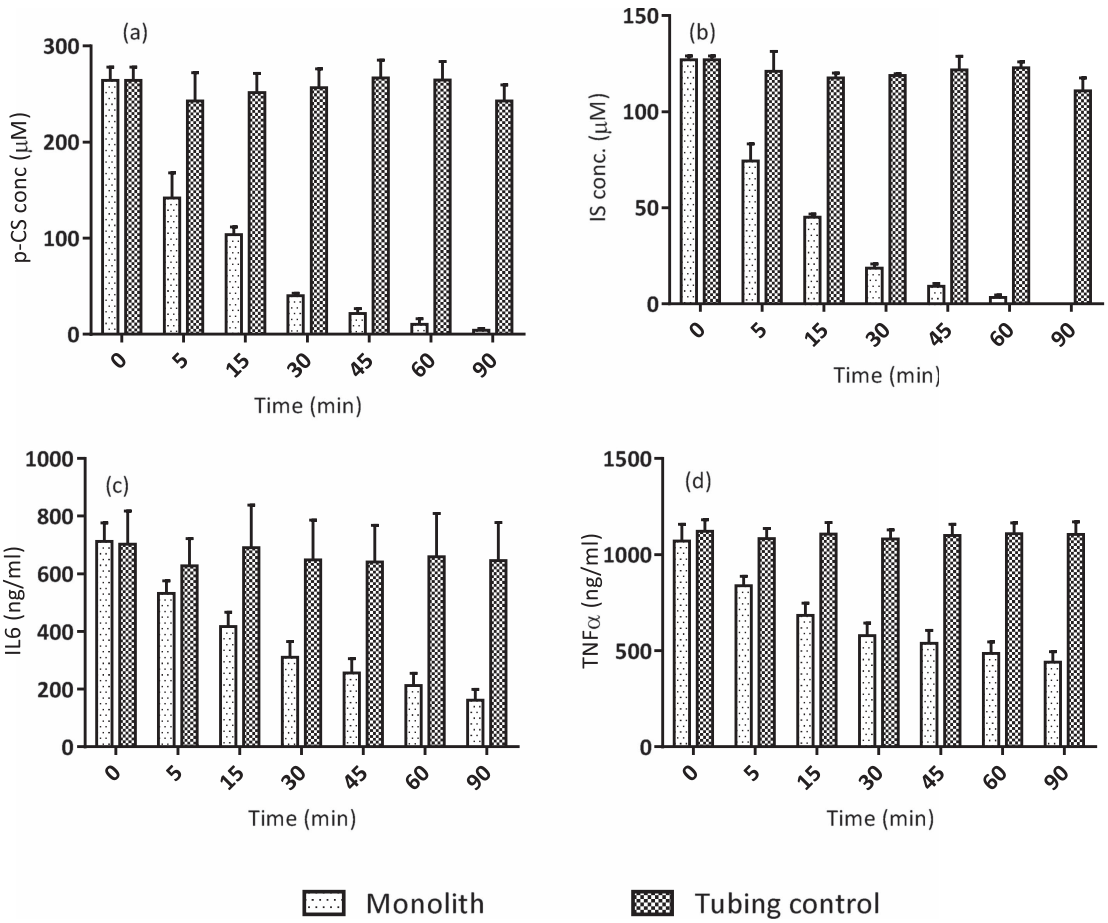


**Figure 5.** Healthy donor blood spiked with IS (125 $\mu$M), p-CS (250 $\mu$M), IL-6 (1000 pg ml$^{-1}$) and TNF(1000 pg ml$^{-1}$) and perfused through the large monoliths at a flow rate of 300 ml min$^{-1}$. (a) IS (b) p-CS (c) IL-6 and (d) TNF-$\alpha$ concentration was significantly reduced following 90 min continuous filtration compared to the tubing only control (SEM±, $n = 3$), $^{*}p < 0.05$.

**Table 1.** Healthy donor blood perfused through the small monoliths at 5 ml min$^{-1}$ for 90 min did not produce significant changes in blood cell count (WBC, RBC, PLT), haematocrit (HCT) and haemoglobin (HB) measures of haemolysis, urea, creatinine, total protein and APPT and INR measures of coagulation compared to tubing only controls (mean ± SD, $n = 3$).

| | Pre-perfusion | Monolith | Tubing | Normal range |
|---|---|---|---|---|
| HB (g l$^{-1}$) | 140.8 ± 16.8 | 137.2 ± 30.4 | 132.8 ± 26.6 | 115–165 |
| WBC × 10$^{9}$ cell ml$^{-1}$ | 7.4 ± 1.5 | 7.4 ± 2.1 | 7.9 ± 2.2 | 4.0–11.0 |
| PLT × 10$^{9}$ cell ml$^{-1}$ | 261 ± 54 | 230 ± 75 | 288 ± 111 | 150–450 |
| RBC × 10$^{12}$ cell ml$^{-1}$ | 4.76 ± 0.59 | 4.57 ± 1.09 | 4.40 ± 0.92 | 3080–5.80 |
| HCT (l l$^{-1}$) | 0.416 ± 0.049 | 0.381 ± 0.095 | 0.365 ± 0.073 | 0.350–0.470 |
| Sodium (mmol l$^{-1}$) | 139 ± 2 | 139.7 ± 0.6 | 137.0 ± 1.7 | 135–146 |
| Potassium (mmol l$^{-1}$) | 4.2 ± 0.2 | 4.1 ± 0.1 | 4.5 ± 0.2 | 3.2–5.1 |
| Urea (mmol l$^{-1}$) | 4.8 ± 1.8 | 3.8 ± 1.4 | 4.8 ± 1.7 | 1.7–8.3 |
| Creatinine ($\mu$mol l$^{-1}$) | 66.7 ± 13.6 | 17.7 ± 5.0 | 69.0 ± 14.7 | 62–106 |
| Total protein (g l$^{-1}$) | 75.7 ± 2.5 | 64 ± 2 | 74.7 ± 1.5 | 66–87 |
| Albumin (g l$^{-1}$) | 46 ± 1 | 39.7 ± 0.6 | 45.3 ± 0.6 | 34–48 |
| Fibrinogen (g l$^{-1}$) | 2.8 ± 0.5 | 2.1 ± 0.4 | 2.8 ± 0.6 | 2.0–4.0 |
| APTT (S) | 1.0 ± 0.1 | 1.0 ± 0.1 | 0.9 ± 0.1 | 0.8–1.2 |
| INR | 0.1 | 1.1 ± 0.1 | 1.0 ± 0.0 | 0.8–1.2 |

administered to the animal to replace blood volume. Plasma biochemistry values showed decreases in albumin and total protein levels, which may have been due to adsorbance by the column, but are also as a result of the haemodilution caused by connection to the saline filled circuit and additional crystalloid boluses. Creatinine values rose at the end of the study, which may indicate a small degree of haemolysis within the circuit resulting from the continued action of the peristaltic pump. Although this difference in

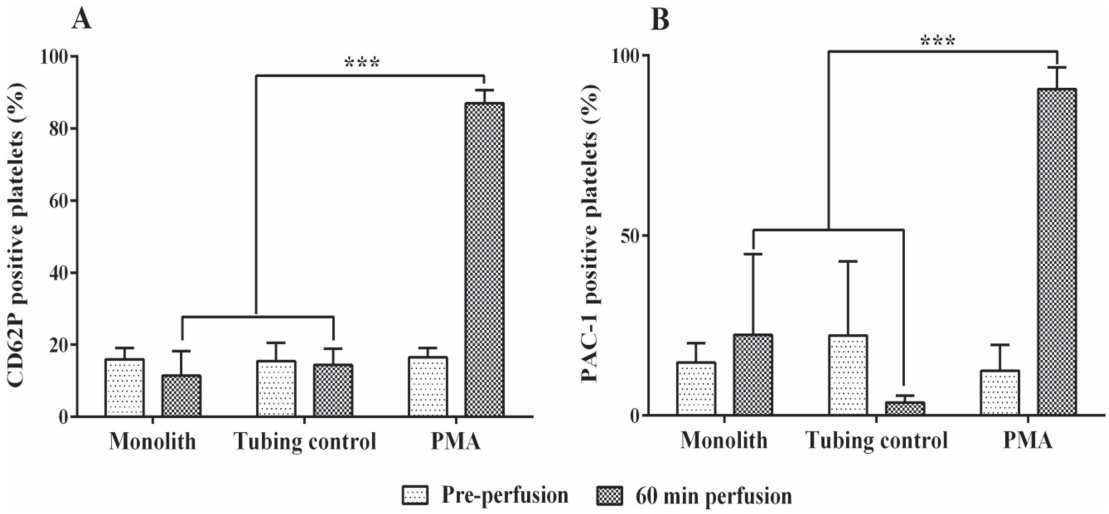


**Figure 6.** Perfusion of healthy donor blood for 90 min through the large monoliths at haemodialysis flow rates did not stimulate platelet activation using (a) PAC-1 and (b) CD62P activation markers compared to tubing only controls. No significant difference in the percentage of PAC-1 and CD62P positive platelets was observed when comparing the monolith and tubing only control. In contrast, the PMA (200 nM) spike induced significant platelet activation (SEM±, $n = 3$), $^{***}p < 0.001$.

creatinine is significant, the values are not excessively high (table 2). Mean arterial blood pressure remained stable throughout the duration of the study, indicating that the animals tolerated the procedure well.

## 4. Discussion

The study provides evidence to support the haemocompatibility and efficacy of a scaleable nanoporous activated carbon monolith device for potential use to augment current haemodialysis therapy. A range of haemocompatibility tests using healthy donor blood samples and a small animal blood perfusion modelling study demonstrated that the monoliths are safe for use in direct blood contact. A novel lignin binder synthesis route was used to successfully scale up the device to a clinically feasible size without reducing adsorptive efficacy for marker protein bound and high molecular weight uraemic toxins. Whilst no previous studies on nanoporous activated carbon monoliths with the porous range demonstrated in this study have been described, *in vitro* study data exists for carbons in bead form include carbide derived carbons, phenolic resin derived activated carbons and carbon incorporated into a mixed matrix hallow fibre membrane form [40–42]. The beads showed some efficacy in spiked plasma studies but offer no solution to the challenges of direct blood contact and pressure drop. Mixed membrane carbon incorporation offers an interesting alternative but may limit contact area for sufficient adsorption of high molecular weight molecules. In mixed membrane form significant IS and PCS removal was reported but no data was reported for high molecular weight species potentially because the membrane cut off limits direct contact. Previous studies comparing synthetic resin derived carbon bead activation burn off and adsorptive efficacy reported reduction of high molecular weight cytokine TNF matching that shown previously for CDCs but data is limited to batch adsorption studies from plasma. Within the current study a phenolic resin derived activated carbon monolith rather than bead based device was shown to reduce IS and PCS levels in spiked whole blood to negligible levels and IL6 and TNF levels by 80% and 60% respectively indicating a scaleable efficacy compared to bead based alternatives. The monolith design solves issues of haemocompatibility and pressure drop across the adsorbent device without resorting to coating with potential subsequent reduction in the molecular weight cut-off and adsorptive profile.

There are many advantages in adapting the activated carbon form to a monolithic structure for direct blood perfusion but also many challenges in maintaining porous profile and adsorptive efficacy. Previous tests using a small monolith prototype and haemodialysis patient blood samples indicated that adsorption of protein bound and middle molecules was dependent on creating nanopores in the 2–100 nm range since adsorption of these solutes in carbon monoliths with narrow nanopores of <2 nm was limited [39]. The challenge in scaling up the monolith was to maintain nanoporosity but also to design the monolith channel parameters to balance maximum adsorption with appropriate internal fluid dynamics [43]. This was achieved in the current device iteration by using a constant 0.3 mm microchannel channel size. A short diffusion distance was provided for access to the internal porous surface area in the walls of the monolith and a micro-channel structure capable of minimising shear stress, maintaining laminar flow and thus reducing red blood cell fragility, haemolysis, platelet activation and thrombus formation. Previous studies with

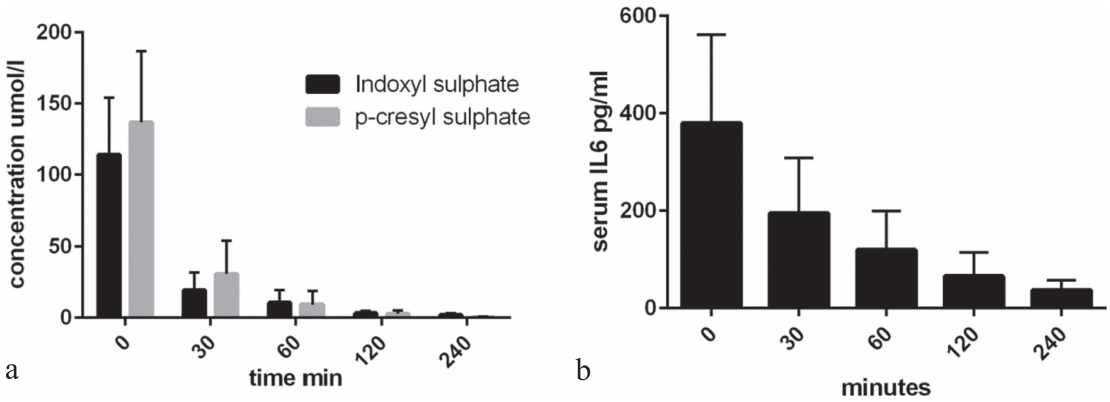


**Figure 7.** (a) Indoxyl sulphate, p-cresyl sulphate (125 $\mu$M IS, 250 $\mu$M p-CS spike) and (b) IL-6 (1 ng ml$^{-1}$ spike) remaining following 240 min spiked blood perfusion through the large monoliths (mean $\pm$ SEM, $n = 8$).

activated carbon granules containing narrow nanopores of <2 nm have highlighted the tendency for excessive pressure drop, platelet consumption, albumin loss and potential for carbon fines release [30]. The introduction of a monolithic design was therefore integral to minimise the tendency for flow irregularities, pressure drop and impact on blood cell fragility, platelet loss and protein adhesion.

Binding of plasma proteins occurs as soon as blood contacts a foreign surface. Dominant plasma proteins albumin, fibrinogen and IgG coat a surface immediately but with a dynamic exchange with other plasma proteins over time [44]. Protein surface coating in the extracorporeal circuit becomes problematic if proteins are denatured and expose activation sites for inflammatory pathway activation or in some cases if a negatively charged surface induces contact activation [44]. Protein surface adhesion may also form a passivating layer, limiting any further inflammatory response. In the current study blood albumin and fibrinogen concentrations were reduced on contact with the monoliths. However, total protein, albumin and fibrinogen concentrations all remained within the normal reference range indicating a non-detrimental, dynamic, adsorptive equilibrium for these dominant plasma proteins over the initial time course of haemodialysis. Adsorption of dominant plasma protein serum albumin (66 kDa) and fibrinogen (340 kDa) did not prevent adsorption of less concentrated high molecular weight IL-6 (28 kDa) and TNF-$\alpha$ (52 kDa), present in picogram quantities, and adsorbed predominantly within the nanoporous domains of the monoliths. The cause of this effect is not clear but could be related to the different hydrophobic domains within the proteins. AC is a hydrophobic adsorbent and it has been reported that the TNF-$\alpha$ trimer undergoes reversible dissociation into three monomeric units in contact with hydrophobic surfaces and therefore smaller molecules of IL-6 and TNF-$\alpha$ monomer (17 kDa) could be adsorbed predominantly within the nanoporous domains of the monoliths inaccessible to albumin [45]. Results confirm no significant impact on total protein, electrolyte and haemolysis parameters using healthy donor blood perfused through the small monoliths over time. Albumin and platelet reduction was slight using the healthy blood samples in contrast to a previous study using post-haemodialysis blood samples where a greater reduction in platelet count and albumin concentration was observed [39]. A number of additional variables including differences in blood sample handling and monolith formulation may have influenced the heightened propensity for haemodialysis blood sample proteins and platelets to adhere but the results also support the premise that haemodialysis patient blood is primed for inflammation.

The haemocompatibility tests were carried out on the small monolith prototypes according to ISO 10993 for blood contacting medical devices assessing platelet activation, granulocyte activation, activation of t-cell intracellular phosphorylation pathways for STAT3 and STAT5 using flow cytometry, complement fragment concentration for C3a, C4a, C5a using ELISA and coagulometry assays measuring pro-thrombin, APPT clotting times and fibrinogen concentration. The signal transducer and activator of transcription (STAT) family are a group of proteins activated by cytokines and growth factors through receptor associated kinase phosphorylation followed by dimerisation, translocation into the nucleus and transcription of genes related to cell proliferation and the inflammatory response. They were used in this study as the earliest indicator of T-cell activation on inflammatory stimulus by the monoliths. Some complement activation and in particular granulocyte activation was detected at the 60 min time point for both monolith and tubing only negative controls. Complement activation is known to occur routinely on exposure to a foreign surface within haemodialysis, cardiopulmonary bypass and apheresis via the alternative pathway [46–48]. The small, cationic peptides C3a, C4a and C5a are anaphylatoxins which are free in the plasma and bind to neutrophils and monocytes to promote ROS production, cytokine release and cell hyper-adhesion. Activation was no

**Table 2.** Naïve rat haemoperfusion data showing the results from blood gas analyses, plasma biochemistry and direct measurement of the mean arterial pressure. Data were analysed using one way ANOVA.

| | Pre-Circuit | 60 min | 120 min |
|---|---|---|---|
| | | Blood gas | |
| pH | 7.4 ± 0.03 | 7.4 ± 0.04 | 7.4 ± 0.07 |
| Haematocrit | 43.3 ± 0.6 | 38 ± 2 | 37.7 ± 3.5 |
| HB (g $dl^{-1}$) | 14.7 ± 0.2 | 13 ± 0.7 | 12.8 ± 1.1 |
| $O_2$ saturation (%) | 96 ± 1.3 | 96.4 ± 1.3 | 96.7 ± 0.9 |
| Sodium (mM) | 135.4 ± 1.7 | 135.4 ± 1.6 | 134.2 ± 1.9 |
| Potassium (mM) | 4.3 ± 0.2 | 4.5 ± 0.3 | 4.6 ± 0.7 |
| Calcium (mM) | 1.3 ± 0.04 | 1.3 ± 0.05 | 1.3 ± 0.03 |
| Chlorine (mM) | 101.5 ± 1.7 | 104.7 ± 2.1 | 104.1 ± 1.8 |
| Glucose (mM) | 14.7 ± 3.2 | 14.2 ± 4 | 16.8 ± 7.2 |
| Bicarbonate (mM) | 26.7 ± 1.1 | 24.9 ± 2.6 | 22.8 ± 3.5$^{*}$ |
| | | Plasma biochemistry | |
| Albumin (g $l^{-1}$) | 34.4 ± 2.8 | 26.9 ± 5.4$^{**}$ | 25.8 ± 4.1$^{***}$ |
| Total protein (g $l^{-1}$) | 49.1 ± 1.8 | 39.5 ± 7.4$^{**}$ | 37.3 ± 4.9$^{***}$ |
| ALT (U $l^{-1}$) | 48.9 ± 11.4 | 36.8 ± 10.4 | 42.6 ± 12.7 |
| AST (U $l^{-1}$) | 67.9 ± 7.4 | 57.6 ± 15.9 | 103 ± 81 |
| Creatinine ($\mu$M) | 20.6 ± 4.5 | 31.1 ± 8.4 | 35.6 ± 11.9$^{**}$ |
| | | Physiological | |
| Mean arterial pressure (mmHg) | 98.7 ± 10.6 | 80.9 ± 17 | 82.2 ± 28.1 |

Note. $^{*}p < 0.05$, $^{**}p < 0.01$, $^{***}p <$ 0.001 versus pre-circuit (time 0) values. Data are shown as mean ± SD, $n = 9$ in each case. Abbreviations: alanine aminotransferase (ALT), aspartate aminotransferase (AST).

more than the tubing only controls and was markedly limited when compared to the zymozan A activated, positive control blood samples, indicating that the artificial surfaces within the perfusion model itself and not the monoliths promoted some activation of inflammatory pathways.

The large monoliths maintained adsorptive efficacy for the uraemic toxins IS and PCS and cytokines IL-6 and TNF-$\alpha$ on scale up and at haemodialysis flow rates with minimal pressure drop. Further work is required to establish breakthrough parameters and the impact of rebound release on adsorption but the current study indicates that an adsorptive equilibrium is maintained over 4 h perfusion time. The broad spectrum adsorptive capacity of the activated nanoporous carbon monoliths for organic molecules indicates that these monoliths will have great capacity to remove other poorly removed protein bound and middle molecule uraemic toxins from the growing family of uraemic toxins known to remain after standard haemodialysis treatments and represented by these marker molecules.

In summary, whilst haemodialysis patients have an immunosuppressive and altered haemostatic balance so that blood cell fragility and inflammatory response on contact with foreign surfaces will inevitably be hypersensitised toward inflammation [49] the results of the current study show that, using healthy donor blood, a nanoporous activated carbon monolith does not exacerbate blood cell activation according to ISO 10993 haemocompatibility measures. Haemocompatibility was also demonstrated using an *in vivo* haemoperfusion safety model where no disruption of blood biochemistry or coagulopathy occurred. The scaled up device maintained the internal nanoporous structure necessary to augment haemodialysis efficacy through broad spectrum adsorption of small, protein bound and high molecular weight uraemic toxins.

## 5. Conclusion

A novel lignin binder synthesis route has been used to synthesise nanoporous activated carbon monoliths with maintained adsorptive capacity for marker protein bound and high molecular weight toxins on scale up and testing at haemodialysis flow rates. These toxins currently remain following haemodialysis and contribute to poor survival related to cardiovascular disease and infection. The carbon monolith is safe and shows good biocompatibility when tested in naive rats. Such a device could potentially be used as an in-line haemoperfusion device to sit in line with and augment the clearance of uraemic toxins poorly removed by standard haemodialysis.

## Acknowledgments

All activated carbon monoliths were synthesised by MAST Carbon International, Jays Close, Viables, Basingstoke, Hampshire, RG22 4BA, UK. This work

is independent research funded by the National Institute for Health Research, UK (Invention for Innovation (i4i), Product Development Awards, II-LA-1111-20003). The views expressed in this publication are those of the author(s) and not necessarily those of the NHS, the National Institute for Health Research or the Department of Health. The work was supported by the NIHR Brighton & Sussex Clinical Research Facility. The University of Brighton and UCL authors acknowledge funding from the People Programme (Marie Curie Actions) of the European Union's Seventh Framework Programme, Industry-Academia Partnerships and Pathways (IAPP) project 'Adsorbent Carbons for the Removal of Biologically Active Toxins' (ACROBAT-Grant agreement no. 286366 FP7-People-2011-IAPP).

## References

[1] Saran R *et al* 2015 US renal data system 2014 annual data report: epidemiology of kidney disease in the United States *Am. J. Kidney Diseases* (1 Suppl.) S1-305 Svii
[2] Ortiz A *et al* 2014 Epidemiology, contributors to, and clinical trials of mortality risk in chronic kidney failure *Lancet* **383** 1831–43
[3] Gansevoort R T *et al* 2013 Chronic kidney disease and cardiovascular risk: epidemiology, mechanisms, and prevention *Lancet* **382** 339–52
[4] Vogelzang J L *et al* 2015 Mortality from infections and malignancies in patients treated with renal replacement therapy: data from the ERA-EDTA registry *Nephrol. Dial. Transpl.* **30** 1028–37
[5] El-Gamal D *et al* 2014 The urea decomposition product cyanate promotes endothelial dysfunction *Kidney Int.* **86** 923–31
[6] Kwan J T C *et al* 1991 Carbamylated hemoglobin, urea kinetic modeling and adequacy of dialysis in hemodialysis-patients *Nephrol. Dial. Transpl.* **6** 38–43
[7] Pietrement C, Gorisse L, Jaisson S and Gillery P 2013 Chronic increase of urea leads to carbamylated proteins accumulation in tissues in a mouse model of CKD *PloS One* **8** e82506
[8] Velasquez M T, Ramezani A and Raj D S 2015 Urea and protein carbamylation in ESRD: surrogate markers or partners in crime? *Kidney Int.* **87** 1092–4
[9] Eloot S, Van Biesen W, Glorieux G, Neirynck N, Dhondt A and Vanholder R 2013 Does the adequacy parameter Kt/V(urea) reflect uremic toxin concentrations in hemodialysis patients? *PloS One* **8** e76838
[10] Duranton F, Depner T A and Argiles A 2014 The saga of two centuries of urea: nontoxic toxin or vice versa? *Semin. Nephrol.* **34** 87–96
[11] Eloot S, Ledebo I and Ward R A 2014 Extracorporeal removal of uremic toxins: can we still do better? *Semin. Nephrol.* **34** 209–27
[12] Vanholder R, Schepers E, Pletinck A, Nagler E V and Glorieux G 2014 The uremic toxicity of indoxyl sulfate and p-cresyl sulfate: a systematic review *J. Am. Soc. Nephrol.* **25** 1897–907
[13] Shafi T *et al* 2015 Free levels of selected organic solutes and cardiovascular morbidity and mortality in hemodialysis patients: results from the retained organic solutes and clinical outcomes (ROSCO) investigators *PloS One* **10** e0126048
[14] Wu I W *et al* 2011 p-cresyl sulphate and indoxyl sulphate predict progression of chronic kidney disease *Nephrol. Dial. Transpl.* **26** 938–47
[15] Sirich T L, Meyer T W, Gondouin B, Brunet P and Niwa T 2014 Protein-bound molecules: a large family with a bad character *Semin. Nephrol.* **34** 106–17
[16] Pletinck A *et al* 2013 Protein-bound uremic toxins stimulate crosstalk between leukocytes and vessel wall *J. Am. Soc. Nephrol.* **24** 1981–94
[17] Neirynck N, Vanholder R, Schepers E, Eloot S, Pletinck A and Glorieux G 2013 An update on uremic toxins *Int. Urol. Nephrol.* **45** 139–50
[18] Duranton F *et al* 2012 Normal and pathologic concentrations of uremic toxins *J. Am. Soc. Nephrol.* **23** 1258–70
[19] Remuzzi G *et al* 2013 Kidney failure: aims for the next 10 years and barriers to success *Lancet* **382** 353–62
[20] Vanholder R, Boelaert J, Glorieux G and Eloot S 2015 New methods and technologies for measuring uremic toxins and quantifying dialysis adequacy *Semin. Dial.* **28** 114–24
[21] Winchester J F 1984 Haemoperfusion in the management of end-stage renal disease *Life Support Syst.* **2** 107–11
[22] Winchester J F *et al* 2002 The next step from high-flux dialysis: application of sorbent technology *Blood Purification* **20** 81–6
[23] Winchester J F *et al* 2004 Sorbents in acute renal failure and end-stage renal disease: middle molecule and cytokine removal *Blood Purification* **22** 73–7
[24] Yatzidis H and Oreopoulos D 1976 Early clinical trials with sorbents *Kidney Int. Suppl.* **7** S215–7
[25] Yatzidis H, Psimenos G and Mayopoulou-Symvoulidis D 1969 Nondialyzable toxic factor in uraemic blood effectively removed by the activated charcoal *Experientia* **25** 1144–5
[26] Yatzidis H, Yulis G and Digenis P 1976 Hemocarboperfusion-hemodialysis treatment in terminal renal failure *Kidney Int. Suppl.* **7** S312–4
[27] Andrade J D, Kopp K, Van Wagenen R, Chen C and Koliff W J 1972 Activated carbon and blood perfusion: a critical review *Proc. European Dialysis and Transplant Association European Dialysis and Transplant Association* vol 9 pp 290–302
[28] Andrade J D, Kunitomo K, Van Wagenen R, Kastigir B, Gough D and Kolff W J 1971 Coated adsorbents for direct blood perfusion: HEMA-activated carbon *Trans.—Am. Soc. Artif. Intern. Organs* **17** 222–8
[29] Bartels O 1978 Hemoperfusion through activated carbon adsorbent in liver-failure and hepatic-coma *Acta Hepato-Gastroenterologica* **25** 324–9
[30] Botella J, Ghezzi P M and Sanz-Moreno C 2000 Adsorption in hemodialysis *Kidney Int. Suppl.* **76** S60–5
[31] Falkenhagen D, Gottschall S, Esther G, Courtney J M and Klinkmann H 1982 *In vitro* assessment of charcoal and resin hemoadsorbents *Contrib. Nephrol.* **29** 23–33
[32] Yang J B, Ling L C, Liu L, Kang F Y, Huang Z H and Wu H 2002 Preparation and properties of phenolic resin-based activated carbon spheres with controlled pore size distribution *Carbon* **40** 911–6
[33] Gun'ko V M *et al* 2008 Structural and adsorption studies of activated carbons derived from porous phenolic resins *Colloid Surf.* A **317** 377–87
[34] Tennison S R 1998 Phenolic-resin-derived activated carbons *Appl. Catal.* A **173** 289–311
[35] Howell C A *et al* 2006 The *in vitro* adsorption of cytokines by polymer-pyrolysed carbon *Biomaterials* **27** 5286–91
[36] Howell C A *et al* 2013 Nanoporous activated carbon beads and monolithic columns as effective hemoadsorbents for inflammatory cytokines *Int. J. Artif. Organs* **36** 624–32
[37] Sandeman S R *et al* 2008 Inflammatory cytokine removal by an activated carbon device in a flowing system *Biomaterials* **29** 1638–44
[38] Sandeman S R *et al* 2005 Assessing the *in vitro* biocompatibility of a novel carbon device for the treatment of sepsis *Biomaterials* **26** 7124–31
[39] Sandeman S R *et al* 2014 An adsorbent monolith device to augment the removal of uraemic toxins during haemodialysis *J. Mater. Sci., Mater. Med.* **25** 1589–97
[40] Pavlenko D *et al* 2016 New low-flux mixed matrix membranes that offer superior removal of protein-bound toxins from human plasma *Sci. Rep.* **6** 34429
[41] Tripisciano C *et al* 2011 Activation-dependent adsorption of cytokines and toxins related to liver failure to carbon beads *Biomacromolecules* **12** 3733–40

[42] Presser V et al 2012 Hierarchical porous carbide-derived carbons for the removal of cytokines from blood plasma *Adv. Healthc. Mater.* **1** 796–800
[43] Gilbert R J et al 2007 Computational and functional evaluation of a microfluidic blood flow device *ASAIO J.* **53** 447–55
[44] van Oeveren W 2013 Obstacles in haemocompatibility testing *Scientifica* **2013** 392584
[45] Kunitani M G, Cunico R L and Staats S J 1988 Reversible subunit dissociation of tumor necrosis factor during hydrophobic interaction chromatography *J. Chromatography* **443** 205–20
[46] Kourtzelis I et al 2010 Complement anaphylatoxin C5a contributes to hemodialysis-associated thrombosis *Blood* **116** 631–9
[47] Kourtzelis I, Rafail S, DeAngelis R A, Foukas P G, Ricklin D and Lambris J D 2013 Inhibition of biomaterial-induced complement activation attenuates the inflammatory host response to implantation *FASEB J.* **27** 2768–76
[48] Rousseau Y, Haeffner-Cavaillon N, Poignet J L, Meyrier A and Carreno M P 2000 *In vivo* intracellular cytokine production by leukocytes during haemodialysis *Cytokine* **12** 506–17
[49] Friedrich B, Alexander D, Janessa A, Haring H U, Lang F and Risler T 2006 Acute effects of hemodialysis on cytokine transcription profiles: evidence for C-reactive protein-dependency of mediator induction *Kidney Int.* **70** 2124–30